Published in final edited form as:
Nanomedicine. 2012 October ; 8(7): 1133–1142. doi:10.1016/j.nano.2012.02.003.

Enhanced Delivery of Gold Nanoparticles with Therapeutic Potential into the Brain using MRI-Guided Focused Ultrasound

Arnold B. Etame, MD[a,#], **Roberto J. Diaz, MD**[a,#], **Meaghan A. O'Reilly, MSc**[b], **Christian A. Smith, PhD**[a], **Todd G. Mainprize, MD**[c], **Kullervo Hynynen, PhD**[b], and **James T. Rutka, MD, PhD**[a,*]

[a]The Hospital for Sick Children – Arthur and Sonia Labatt Brain Tumour Research Centre, Division of Neurosurgery, Department of Surgery, and Department of Laboratory Medicine & Pathobiology at the University of Toronto, Toronto, Canada

[b]Division of Imaging Research at Sunnybrook Research Institute, and Department of Medical Biophysics at the University of Toronto, Toronto, Canada

[c]Division of Neurosurgery, Sunnybrook Hospital, University of Toronto, Toronto, Canada

Abstract

The blood brain barrier (BBB) is a major impediment to the delivery of therapeutics into the central nervous system (CNS). Gold nanoparticles (AuNPs) have been successfully employed in multiple potential therapeutic and diagnostic applications outside the CNS. However, AuNPs have very limited biodistribution within the CNS following intravenous administration. Magnetic resonance imaging guided focused ultrasound (MRgFUS) is a novel technique that can transiently increase BBB permeability allowing delivery of therapeutics into the CNS. MRgFUS has not been previously employed for delivery of AuNPs into the CNS. This work represents the first demonstration of focal enhanced delivery of AuNPs into the CNS using MRgFUS in a rat model both safely and effectively. Histologic visualization and analytical quantification of AuNPs within the brain parenchyma suggest BBB transgression. These results suggest a role for MRgFUS in the delivery of AuNPs with therapeutic potential into the CNS for targeting neurological diseases.

Keywords

Nanoparticles; blood brain barrier; focused ultrasound; central nervous system; magnetic resonance imaging

Background

Therapeutic nanoparticles (1 – 100 nm in diameter) have emerged as promising tools in nanomedicine.[1] Gold nanoparticles (AuNPs) are bio-inert and nontoxic which are important features of biocompatible nanomaterials.[2–4] AuNPs have been successfully employed in cancer targeting,[5–9] imaging,[10] delivery of therapeutics,[11] gene targeting,[12] as well as

*Corresponding Author: James T. Rutka, MD, PhD, The Arthur and Sonia Labatt Brain Tumor Research Centre, The Hospital for Sick Children, Department of Neurosurgery, University of Toronto, M5S 3G9 (Canada), james.rutka@sickkids.ca.
#Both authors contributed equally to the study.

thermal ablation of tumors.[13–20] These novel targeted diagnostic and therapeutic applications could have significant implications within the central nervous system (CNS) in the treatment of neurological disorders where targeted therapies are most highly desirable in light of toxicity vulnerabilities.

However, the blood brain barrier (BBB) provides a significant impediment to targeted AuNP applications within the CNS. The endothelial cells of brain capillaries are uniquely interconnected by intercellular protein bridges, called tight junctions, which block the free diffusion of small molecules from the circulation into the brain parenchyma. In effect, normal brain capillaries may exclude nanoparticle uptake into the brain that is driven by hydrostatic and osmotic gradients, while passive or active transcellular uptake can still occur.

AuNP data from several biodistribution studies in animals with intact BBB highlight delivery challenges associated with the BBB.[21–24] When De Jong *et al*. delivered intravenous AuNP with size ranges between 10 nm to 250 nm into rats, they could only detect gold in the brains of animals treated with the 10 nm AuNP.[21] Moreover only 0.3% of the delivered dose was found within the brain in comparison to 46.3% within the liver.[21] Similarly, Sonavane *et al*. detected gold within the brain of mice treated with either 15 nm or 50 nm AuNPs at very high doses of 1g/kg, but not with 100 nm or 200 nm AuNPs.[23] However, the reported amounts represented less than 0.08% of the administered dose.[23] Even more intriguing, when polyethylene glycol (PEG) coated AuNPs with sizes of 10 nm and 50 nm were employed by Trentyuk *et al*. in rats, they did not measure any significant amount of gold in the brain.[22] Most recently Lasagna-Reeves *et al*. examined the biodistribution of daily intra-peritoneal delivery of 12.5 nm AuNPs in mice over 8 days. The AuNP biodistribution within the brain was extremely limited in comparison to the liver or spleen even after serial AuNP administration.[24] The above studies clearly underscore the size-dependent and limited nature of AuNP delivery into the CNS for which the intact BBB is the explanation. Therefore, strategies that result in transient permeability of the normal BBB could potentially enhance the biodistribution of therapeutic AuNPs into the brain for the treatment of neurological diseases wherein the BBB is intact. Such strategies should ideally entail safe and reversible transient increases in BBB permeability to AuNP therapeutics while simultaneously limiting the influx of toxins into the CNS.

MRI-guided focused ultrasound (MRgFUS) is a novel technique that selectively and focally disrupts the BBB, thereby increasing its permeability to macromolecules into regions of interest within the brain.[25–29] Intravenously injected lipid-shell perfluorocarbon microbubbles assist with BBB disruption. This noninvasive technique also increases BBB permeability in a transient, non-toxic and reversible manner.[25, 29] The BBB disruption induced with MRgFUS typically lasts for 4–6 hrs and has been shown to allow transit of macromolecules up to 150 kDa into the brain in mouse and rat models.[30–32] Magnetic resonance imaging (MRI) is used to select the region of brain to be targeted by focused ultrasound and also to visualize the extent of BBB disruption. The feasibility of MRgFUS mediated delivery of macromolecules and therapeutics into the brain has been successfully demonstrated in several studies.[33–39] However, the application of MRgFUS to enhance delivery of AuNP-based nano-carriers into the CNS has not been previously described. Such

an application could potentially have significant implications especially given the BBB limitations of CNS biodistribution of intravenously administered AuNPs.

Hence, given the significant therapeutic and diagnostic potential of AuNPs within the CNS in conjunction with the selective and targeted capabilities of FUS to overcome delivery challenges across the BBB, this study was undertaken in order to ascertain if FUS could enhance the clinical utility of AuNPs for subsequent CNS applications. We hypothesized that FUS could alter the conventional biodistribution of AuNPs leading to enhanced delivery within the brain. Accordingly, we assessed the delivery of 50 nm polyethyleneglycol coated AuNPs (PEG-AuNPs) across the BBB with FUS in a rat model since this AuNP size was previously shown to have the best intracellular uptake kinetic profile,[40–42] For the first time, we demonstrate significant enhanced delivery of AuNPs into the brain parenchyma using focus ultrasound. We also conclusively address the issue of AuNP localization within the CNS by detecting AuNPs within brain parenchyma using silver enhancement histology. Lastly we show that our MRgFUS scheme can result in delivery into the CNS that offset the traditional miss-match in AuNP biodistribution between the brain and liver. Taken together, these results suggest a potential role for MRgFUS for future delivery of AuNP-based therapeutics into the CNS.

Methods

Characterization of AuNPs

Size-certified 50 nm AuNPs coated with thiolated PEG (MW 2000) were purchased from Nanocs, New York. AuNPs were further characterized with TEM for core diameter assessment and also with agarose gel electrophoresis to document PEG coverage. For the TEM assessment, samples were loaded onto carbon-coated copper grids and images were obtained using Hitachi HD2000 STEM (Hitachi Corp). Particle sizes were measured from TEM using Image J software. For the agarose gel characterization, the differential electrophoretic mobilities of PEG coated and non-PEG coated AuNPs were assessed. Samples were run on a 1% agarose gel at 120 mV for 30 minutes and the gel was subsequently photographed.

MRgFUS delivery scheme

This study was conducted with the approval of the Sunnybrook Hospital Research Institute Animal Care Committee (Animal Use Protocol #10–281) and in compliance with the guidelines established by the Canadian Council on Animal Care and the Animals for Research Act of Ontario, Canada. Wistar rats weighing 243–272 g (Charles River, Quebec, Canada), were anaesthetized with inhaled isofluorane for induction. Hair over the dorsal aspect of the skull was shaved and dilapidated. An angio-catheter was inserted into the tail vein. Maintenance anaesthesia was then achieved with ketamine (40–50 mg/kg) and xylazine (10 mg/kg) and the animal was removed from isofluorane exposure for 5 minutes prior to the start of the experiment. The animal was placed in a supine position with the exposed scalp immersed in degassed water and with its limbs secured (Figure 1). The degassed water serves as a conduction media for ultrasound waves emitted from a spherically focused transducer constructed in-house (558 kHz, FN=0.8, 10 cm aperture).[43]

The transducer is mounted on a MRI-compatible 3D positioning system similar in principle the one described previously.[43] Magnetic resonance imaging (MRI) of the animal brain was obtained prior to and after focused ultrasound BBB disruption. The images were obtained using a 1.5 T MRI (Signa 1.5 T, General Electric) set at ETL = 4, FOV = 6 cm × 6 cm, slice thickness = 1 mm, 128 × 128 with T2W FSE parameters being TE = 61.7 ms, TR = 2000 ms, and T1W FSE parameters being TE = 10 ms, TR = 500 ms. Gadodiamide was given at a dose of 0.2 mL/kg prior to and after focused ultrasound BBB disruption to assess the changes in brain vascular permeability. After baseline imaging,animals received 14 mg/kg (by weight of $HAuCl_4$) of 50nm PEG-AuNPs (Nanocs, Inc., New York, NY, U.S.A.), followed immediately by 0.02 mL/kg Perflutren lipid microspheres (Definity®, Lantheus Medical Imaging, Inc., N. Billerica, MA, U.S.A) diluted 10:1 in normal saline. The tail vein angio-catheter lines were immediately flushed with saline after nanoparticle and microbubble administration. Focused ultrasound was delivered at the start of microbubble infusion. The target selected for sonication was the parasagittal right frontal lobe. This region was covered using two lines of 4 focal point sonications spaced anterior to posterior in the hemisphere at 2 mm intervals. The two sets of 4 focal point sonications were separated in time by 5 minutes with Definity® administration immediately prior to each sonication set. PEG-AuNP were only administered once prior to the first sonication. The BBB was disrupted using 0.42W acoustic power (approximately 0.26 MPa peak acoustic pressure) in 10 ms bursts at 1 Hz periodic repeat frequency for 2 minutes.

Experimental Design

Animals served as their respective controls for MRgFUS in that the right hemisphere was always sonicated by FUS while the non-treated left hemisphere served as the control. AuNPs were always administered prior to FUS sonication. Animals were observed for 2 hrs and then euthanized with 120mg/kg pentobarbital sodium (Euthanyl®, BIMEDA-MTC Animal Health Inc, Cambridge, Canada) via intraperitoneal injection. Blood was collected through cardiac puncture. The liver, spleen, kidney, stomach, and brain were collected. The right and left hemispheres of the brain were separated along the midline interhemispheric fissure, photographed and stored separately. The isolated tissues and blood from animals (n=5) were weighed accurately and were stored at −20 °C until gold content analysis. Another set of Wistar rats weighing 392 to 451 gm were randomly assigned to receive intravenously either 5 mg (by weight of $HAuCl_4$) of AuNPs (n=4) or an equivalent saline volume (n=3) immediately prior to sonication. These animals were allowed to recover from anaesthetic and were maintained in a monitored animal facility. During recovery blow-by oxygen at 10 L/min was administered if it was felt the animals showed signs of respiratory distress such as increased work of breathing, excess secretions, or crackles. Animals were observed on a daily basis for signs of neurological impairment including involuntary limb movement, lethargy, weakness, dehydration, and weight loss. Two doses of Buprenorphine 0.125 mg/kg (University of McGill) were administered 12 hrs apart during recovery. The animals were allowed to survive for 4 weeks and then sacrificed for assessment of delayed effects of MRgFUS application with and without AuNP administration.

Histology and silver-augmentation for in-situ AuNP detection

Animals underwent light microscopic histological evaluations of the brain, spleen, liver and kidney at 2 h (n=1) and 5 days (n=1) and of the brain at 4 weeks (n=4) after AuNP administration. Tissue preparation and silver-augmentation were carried out by the Pathology Department at the Hospital for Sick Children in Toronto, Canada. Tissues fixed with 3.7% formalin (Sigma-Aldrich) were embedded in paraffin blocks, and then sliced into 5 μm sections. For assessment of delayed pathological changes in the brain at 4 weeks the whole brain was isolated, fixed with 3.7% formalin, and 10 sections spaced 500 μm apart in the mid axial plane on each brain were examined for evidence of necrosis, hemorrhage, vacuolation, neuronal loss, and inflammation. The silver-enhancement protocol from Jackson ImmunoResearch Laboratories, Inc (West Grove, PA, USA) was employed on dewaxed mounted sections of brain, liver, spleen, and kidney. Silver enhancement was quenched after 30–40 minutes, and sections were then counter-stained with hematoxylin and eosin (H&E). Representative tissue sections were also stained with H&E, but without any silver enhancement as controls.

Measurement of brain and organ distribution of AuNP

Gold was extracted from the harvested organs using protocols previously described by Niidome and colleagues.[45] Briefly, the harvested organs and blood were digested in aqua regia (3:1 HCL/HNO_3) in screw top glass vials. Subsequent evaporation of the aqua regia produced a residue which was dissolved in 3 mL of 0.5N HCl and analyzed by ICP-MS. The ICP-MS analysis was conducted by Maxxam Analytics, Burnaby, British Columbia, Canada.

Statistical Analysis

Statistical analysis was performed using PASW Statistics 18 software. Normality of data was confirmed using the Kolmogorov–Smirnov test with Lilliefor's correction. A two-tailed, paired t-test (α=0.05, n=5) was used to determine if the difference in gold content between right and left hemispheres was statistically significant. One-way analysis of variance (α=0.05, n=5) was used to determine if the difference in gold content between organs was statistically significant. Homogeneity of variances was assured with the Levene statistic.

Results

Characterization of AuNPs

Polyethylene glycol (PEG) coating of gold nanoparticles was confirmed with agarose gel electrophoresis. We examined the electrophoretic mobilities of PEG AuNPs and bare AuNPs. In addition to the 50 nm diameter particles, we also\ employed 10 nm diameter particles as a control. Polyethylene g lycol-coated AuNPs showed no electrophoretic mobility compared to AuNPs stabilized with citrate (Figure 2A). However, the overall differential mobility of 10 nm AuNPs (control) was significantly higher than for the 50 nm particles (Figure 2A). The pegylated AuNPs had a dark brown coloration (Figure 2C). AuNPs were also assessed for core size by transmission electron microscopy (TEM). The TEM demonstrated monodisperse spherical AuNPs (Fig. 2B).

MRgFUS Disruption of BBB

The schematic for the MRgFUS system is demonstrated in Figure 1. For each animal only the right hemisphere was sonicated in the presence of circulating microbubbles. Following micro-bubble assisted disruption of the BBB, MRI gadolinium contrast agent was given and an MRI scan was obtained. Contrast-enhanced T1-weighted (Figure 3A) did not show gadolinium extravasations prior to focal BBB disruption. The corresponding T2-weighted MRI (Figure 3B) prior to BBB disruption was normal. Following MRgFUS, extravasations of gadolinium was demonstrated within the right hemisphere confirming BBB disruption (Figure 3C). Some areas of BBB disruption showed corresponding signal changes on T2-weighted images (Figure 3D). The disruption was carried out within the paramedian aspect of the hemisphere and extended from the convexity to the base of the skull as demonstrated in the contrast enhanced sagittal, and coronal T1-weighted images (Figure 3E–F). A non-homogeneous contrast enhancement pattern within the ultrasound focus was observed in 3 of 5 animals in which orthogonal magnetic resonance imaging was performed. The average spacing between peak contrast intensity in these animals 0.16 cm (n=3) corresponded well with the half wavelength of the ultrasound (approximately 0.13 cm), suggesting standing wave influence.

Gross pathological examination of the brain

The gross pathology of the brain was examined 2 hours after BBB disruption. The sonicated right and non-sonicated left hemispheres were sectioned along the midline interhemispheric fissure. Examination of the medial aspects of the hemispheres clearly demonstrates evidence of punctate extravasations seen as reddish-brown deposits within the sonicated hemisphere whereas the non-sonicated hemisphere has a normal appearance (Supplementary Figure 1A in Supporting Information). The extravasations represent disruption of the BBB in focal areas within the treated hemisphere. This was further confirmed by silver enhancement histology (Supplementary Figure 1B in Supporting Information).

Histological examination of the brain

The hemispheres were examined by H&E histology as well as silver augmentation techniques. Silver augmentation is a well-established technique for visualizing AuNPs in H&E sections. Coronal and axial sections were examined. A representative coronal section at low magnification shows (arrow) areas of extravasations within the sonicated right hemisphere but not within the non-sonicated left hemisphere (Figure 4A). Silver augmentation in combination with H&E demonstrates AuNPs within the perivascular spaces as well as within the brain parenchyma (arrow) following MRgFUS treatment of the right hemisphere (Figure 4B). AuNPs can be visualized (arrow) approximately 150 μm from the site of disruption (Figure 4B). On the contrary, the AuNPs within the non-sonicated left hemisphere localized mainly within intravascular compartment without any appreciable localization within the brain parenchyma (Figure 4C). At 4 weeks after focused ultrasound application to the right hemisphere 2 of 7 animals demonstrated small resolving subcortical hemorrhage (Supplementary Figure 2A in Supporting Information). However, no isolated areas of necrosis, inflammation, or neuronal loss were found (Supplementary Figure 2B in

Supporting Information). Remnant perivascular and parenchymal AuNPs were present 4 weeks after MRgFUS delivery (Supplementary Figure 2C in Supporting Information)).

Histological examination of the liver, spleen, and kidney

Histological sections of liver, spleen, and kidney of treated animals were performed in order to assess for any significant changes. There were no histological abnormalities noted (Supplementary Figure 3A–C in Supporting Information). Using silver augmentation, AuNPs were visualized within the spleen, liver, and kidney. The most significant AuNPs visualization was noted within the spleen, which corresponded to the maximum gold concentration per gram of organ tissue recorded by inductively coupled mass spectroscopy (ICP-MS) amongst all the organs tested (Figure 5).

Quantitative assessment of AuNP content within the brain

Animals were intravenously given 50 nm PEG-AuNPs (14mg/kg) via the tail vein and the right hemisphere was sonicated with MRgFUS. Two hours after BBB disruption animals were euthanized and each hemisphere was assessed for gold content by ICP-MS. The ICP-MS data show a significant difference between the gold content of the sonicated right hemisphere versus the non-sonicated left hemisphere. MRgFUS treatment of the right hemisphere resulted in over 3-fold enhancement of AuNP delivery when compared to the left hemisphere brain (1593 ± 190 ng Au/gm brain S.E.M. Right Hemispheres versus 474 ± 46 ng Au/gm brain S.E.M. Left Hemispheres, $P = 0.007$) (Figure 5).

Biodistribution of AuNPs outside the CNS

The biodistribution of 50 nm PEG-AuNP outside the CNS was also assessed at 2 hours after BBB disruption similar to the assessment for the CNS content (brain in particular). The gold content of the spleen, liver, kidney, and blood for each animal were measured by ICP-MS and reported in ng/gm of organ. The highest amount of gold was seen within the spleen (20760 ± 4097 ng/gm, S.E.M), followed by blood (4796 ± 4032 ng/gm S.E.M), kidney (3914 ±1225 ng/gm, S.E.M) and liver (1685 ± 990 ng/gm, S.E.M) (Figure 6). Gold content was significantly different between organs ($df = 3$, $F = 43.058$, $P < 0.001$).

Discussion

The intact BBB is a major impediment to the delivery of therapeutics into the CNS for the treatment of neurological disorders. Therefore, novel delivery strategies that can overcome the traditional challenges associated with the BBB have the potential to significantly impact the diagnosis and subsequent targeting of disease processes within the CNS. Nano-delivery platforms serve as attractive carriers in light of their small size as well as their unique abilities to traverse biological membranes. In particular, AuNP platforms have been employed in multiple practical therapeutic and diagnostic applications outside the CNS.[6–12, 14–19] However, there are significant limitations in CNS bioavailability of AuNPs following intravenous administration based on animal biodistribution studies.[21–24] Therefore, in order to improve applicability of AuNP delivery platforms within the CNS, we employed MRgFUS - a novel technique that has been shown to transiently disrupt the BBB and potentially deliver therapeutics into the brain.[33–39]

To the best of our knowledge, this study represents the first demonstration of focal enhanced delivery of AuNPs into the cerebral hemisphere. We used MRgFUS parameters that had been previously optimized and well tolerated in small animals.[43] The study was designed such that each animal would serve as its own control. The right hemisphere of the brain was sonicated with MRgFUS while the left hemisphere was not, and served as control. By quantifying the amount of gold within both hemispheres of the brain, we were able to show that MRgFUS alters the AuNP biodistribution within the sonicated right hemisphere to comparable levels like the liver within 2 hrs of administration of AuNP. Hence a significant amount of AuNPs can be delivered into the brain with MRgFUS within a short period of time, which would not have been otherwise possible by conventional means. In addition, MRgFUS appeared to limit the fraction of AuNPs that would have otherwise been sequestered in the spleen and liver. Using silver augmentation techniques, we detected AuNPs within the brain parenchyma of the MRgFUS treated right hemisphere. There were areas of red blood cells (RBCs) extravasation in conjunction with AuNPs, but we also observed gold within the brain parenchyma even in the absence of RBC extravasation in the acute (2 hr) and subacute period (4 weeks). This would suggest that AuNPs could be safely delivered across the BBB without RBC extravasation. Areas of red blood cell extravasation in the region of BBB disruption clustered in white matter tracts, which may be indicative of regional variability in the brain vasculature response to a set peak sonication pressure or effects of non-homogeneity in microbubble size. Furthermore, we were able demonstrated that FUS can deliver AuNPs to distances as far as 150 μm from the transiently disrupted BBB without any associated extravasation of RBCs (Figure 4). This is particularly important since therapeutics can be delivered further into the brain thereby overcoming diffusion-related limitations within the brain parenchyma. The extensive migration of AuNPs into the brain parenchyma could be attributed to the combined ballistic effects of bubble oscillation, radiation pressure and acoustic streaming. In addition, enhanced diffusion across the extracellular space following BBB disruption could also play a secondary role.

The exact localization of AuNPs within normal brain, parenchyma versus intra-vascular space, has not been defined previously. We have observed AuNPs in the capillaries within normal brain and extravasation of AuNPs into the brain parenchyma in the region of focused BBB disruption. Parenchymal localization of AuNPs has significant therapeutic relevance because if AuNPs are restricted to the intra-vascular space, then that would of necessity limit their clinical utility for targeted delivery application into the brain parenchyma. We demonstrated both peri-vascular and intra-parenchymal localization of AuNPs with the MRgFUS-treated right hemisphere suggesting that the AuNPs have transgressed the BBB. On the contrary, the non-treated left hemisphere had AuNP localized to the intravascular space and AuNPs were cleared from the intravascular spaces by 4 weeks. Interestingly this non-sonicated hemisphere also had measurable AuNP content by ICP-MS although there was no detectable gold within the brain parenchyma. These findings suggest that the ICP-MS quantified AuNP content from previous biodistribution studies might have as well been reflective of intravascular space localization as opposed to localization within the brain parenchyma as has been previously reported in prior biodistribution studies.[21–24] Lastly, MRgFUS opened the BBB in focal areas as is evident from the AuNP deposition within the brain. Focal opening of the BBB is more advantageous compared to the non-focal

widespread BBB disruption that is encountered with osmotic agents employed for a similar purpose. MRgFUS therefore translates into targeted delivery, which in itself is a necessary requirement for advancing AuNP platform therapeutics within the CNS to treat neurological disorders.

Given the potential for induction of seizures, hemorrhage, and cerebral edema after BBB disruption we observed a set of rats in which received MRgFUS disruption with the same ultrasound parameters as the group of animals in which gold uptake was quantified. The survival of these animals (n=7) to 4 weeks with no evidence of seizures or neurological deficit shows that focal transient disruption of the BBB with MRgFUS was safe. Delivery of AuNPs into the CNS by MRgFUS in four of these animals did not result in any neurological deficit or pathologic changes on brain histology secondary to vascular occlusion or induction of inflammatory response. We did however observe resolving hemorrhagic foci in the sonicated hemisphere in some animals. From our previous experience, the intensity of gadolinium enhancement can be a marker for the degree of BBB disruption. Comparing the peak intensity observed in our study to prior studies suggests that we may be able to reduce the sonication peak pressure even further, allowing transient blood brain barrier disruption with lower risk of immediate complication such as hemorrhage.

Furthermore, we were also interested in the effects of MRgFUS on the biodistribution profile of the AuNPs. Traditionally, AuNPs concentrate in the liver and spleen from systemic delivery. This effect appears to be less with PEG coated AuNPs. As expected, most of our AuNPs were found in the spleen followed by the blood after 2 hrs. However, the amount of AuNPs within the liver was within a tenth of magnitude comparable to the MRgFUS sonicated right hemisphere when normalized for the mass of the organ. This would at least suggest that MRgFUS mediated-delivery significantly minimizes the traditional AuNP biodistribution miss-match that exists between the liver and brain. Furthermore since this was assessed only at 2 hrs post treatment and a substantial amount of AuNP was still present in blood, it is possible that additional AuNPs would have accumulated in sonicated hemisphere brain over time. Moreover, because we normalized our AuNP values based on the entire right hemisphere mass as opposed to the focal volume of BBB disruption within the hemisphere, we may have underestimated the relative amount AuNPs delivered into the region of brain with BBB disruption. Ideally, one would acquire a more accurate representation of the enhanced focal delivery of AuNP by normalizing the gold content to the volume of brain that demonstrates BBB disruption after sonication. However, volumetric image acquisition in our system was limited due to resolution constraints associated with imaging the small brain of rats. Another potential approach to circumventing the effects of the spleen and liver on AuNP biodistribution would be intra-arterial administration via the carotid artery.

A major limitation of conventional delivery of large molecules such as 50 nm AuNPs is compromised diffusion within the extracellular spaces of the brain. The size constraint of normal brain extracellular space has previously been predicted at 38 – 64 nm based on in vivo diffusion analysis with quantum dots and dextrans.[44] Nonetheless, we employed 50 nm AuNPs since this particle size has been shown to have the best intracellular uptake kinetic profile,[40–42] which is advantageous for therapeutic delivery. Through MRgFUS we were

able to circumvent diffusion-related limitations by demonstrating focal delivery of 50 nm AuNPs across the blood-brain barrier further into brain parenchyma. Once focally delivered, the favorable uptake kinetics of 50 nm AuNPs can be exploited for intracellular delivery of chemotherapy, small interfering RNAs (siRNAs), peptides and other macromolecules of therapeutic value. In addition, given the successful delivery of 50nm AuNPs, one should anticipate marked enhanced delivery of smaller particles with optimal passive diffusion profiles.

In summary, our work represents the first demonstration of focal enhanced delivery of AuNPs with therapeutic potential into the cerebral hemisphere using MRgFUS in a rat model. Based on silver enhancement histology, this work also provides the first direct evidence of localization of AuNPs within the brain parenchyma suggesting BBB transgression. Lastly, we also show that MRgFUS could significantly minimize the AuNP biodistribution mismatch that traditionally exists between the liver and brain. Taken together, these results suggest a potential role for MRgFUS in the delivery of AuNPs with therapeutic potential into the CNS for targeting neurological disorders.

Supplementary Material

Refer to Web version on PubMed Central for supplementary material.

Acknowledgments

We thank Shawna Rideout (animal care), Alex Garces (animal care), and Yuexi Huang (MRgFUS application) from the Imaging Department at Sunnybrook Research Institute (Toronto, Ontario, Canada) for their technical expertise and advice. We also thank Huimin Wang from the Department of Pathology at The Hospital for Sick Children (Toronto, Ontario, Canada) for technical expertise with H&E and silver-enhancement histology.

We acknowledge the Canadian Institutes of Health Research (CIHR) MOP-74610, Congress of Neurological Surgeons Penfield Award, Canadian Cancer Society Research Institute, Brain Tumour Foundation of Canada, Brainchild – Canada, Canadian Research Chairs program, and National Institute of Health (NIH) grant No. EB003268 for financial support.

References

1. Kim BY, Rutka JT, Chan WC. Nanomedicine. N Engl J Med. 2010; 363:2434–2443. [PubMed: 21158659]
2. Connor EE, Mwamuka J, Gole A, Murphy CJ, Wyatt MD. Gold nanoparticles are taken up by human cells but do not cause acute cytotoxicity. Small. 2005; 1:325–327. [PubMed: 17193451]
3. Male KB, Lachance B, Hrapovic S, Sunahara G, Luong JH. Assessment of cytotoxicity of quantum dots and gold nanoparticles using cell-based impedance spectroscopy. Anal Chem. 2008; 80:5487–5493. [PubMed: 18553941]
4. Glazer ES, Zhu C, Hamir AN, Borne A, Thompson CS, Curley SA. Biodistribution and acute toxicity of naked gold nanoparticles in a rabbit hepatic tumor model. Nanotoxicology. 2010
5. Choi CH, Alabi CA, Webster P, Davis ME. Mechanism of active targeting in solid tumors with transferrin-containing gold nanoparticles. Proc Natl Acad Sci U S A. 2010; 107:1235–1240. [PubMed: 20080552]
6. Paciotti GF, Myer L, Weinreich D, Goia D, Pavel N, McLaughlin RE, Tamarkin L. Colloidal gold: a novel nanoparticle vector for tumor directed drug delivery. Drug Deliv. 2004; 11:169–183. [PubMed: 15204636]
7. Hainfeld JF, Slatkin DN, Smilowitz HM. The use of gold nanoparticles to enhance radiotherapy in mice. Phys Med Biol. 2004; 49:N309–N315. [PubMed: 15509078]

8. Mukherjee P, Bhattacharya R, Wang P, Wang L, Basu S, Nagy JA, Atala A, Mukhopadhyay D, Soker S. Antiangiogenic properties of gold nanoparticles. Clin Cancer Res. 2005; 11:3530–3534. [PubMed: 15867256]
9. Brown SD, Nativo P, Smith JA, Stirling D, Edwards PR, Venugopal B, Flint DJ, Plumb JA, Graham D, Wheate NJ. Gold nanoparticles for the improved anticancer drug delivery of the active component of oxaliplatin. J Am Chem Soc. 132:4678–4684. [PubMed: 20225865]
10. Wang H, Huff TB, Zweifel DA, He W, Low PS, Wei A, Cheng JX. In vitro and in vivo two-photon luminescence imaging of single gold nanorods. Proc Natl Acad Sci U S A. 2005; 102:15752–15756. [PubMed: 16239346]
11. Kim CK, Ghosh P, Rotello VM. Multimodal drug delivery using gold nanoparticles. Nanoscale. 2009; 1:61–67. [PubMed: 20644861]
12. Wijaya A, Schaffer SB, Pallares IG, Hamad-Schifferli K. Selective release of multiple DNA oligonucleotides from gold nanorods. ACS Nano. 2009; 3:80–86. [PubMed: 19206252]
13. Glazer ES, Zhu C, Massey KL, Thompson CS, Kaluarachchi WD, Hamir AN, Curley SA. Noninvasive radiofrequency field destruction of pancreatic adenocarcinoma xenografts treated with targeted gold nanoparticles. Clin Cancer Res. 2010; 16:5712–5721. [PubMed: 21138869]
14. Cheng Y, A CS, Meyers JD, Panagopoulos I, Fei B, Burda C. Highly efficient drug delivery with gold nanoparticle vectors for in vivo photodynamic therapy of cancer. J Am Chem Soc. 2008; 130:10643–10647. [PubMed: 18642918]
15. Hirsch LR, Stafford RJ, Bankson JA, Sershen SR, Rivera B, Price RE, Hazle JD, Halas NJ, West JL. Nanoshell-mediated near-infrared thermal therapy of tumors under magnetic resonance guidance. Proc Natl Acad Sci U S A. 2003; 100:13549–13554. [PubMed: 14597719]
16. Visaria RK, Griffin RJ, Williams BW, Ebbini ES, Paciotti GF, Song CW, Bischof JC. Enhancement of tumor thermal therapy using gold nanoparticle-assisted tumor necrosis factor-alpha delivery. Mol Cancer Ther. 2006; 5:1014–1020. [PubMed: 16648573]
17. Huang X, Jain PK, El-Sayed IH, El-Sayed MA. Plasmonic photothermal therapy (PPTT) using gold nanoparticles. Lasers Med Sci. 2008; 23:217–228. [PubMed: 17674122]
18. Bernardi RJ, Lowery AR, Thompson PA, Blaney SM, West JL. Immunonanoshells for targeted photothermal ablation in medulloblastoma and glioma: an in vitro evaluation using human cell lines. J Neurooncol. 2008; 86:165–172. [PubMed: 17805488]
19. Schwartz JA, Shetty AM, Price RE, Stafford RJ, Wang JC, Uthamanthil RK, Pham K, McNichols RJ, Coleman CL, Payne JD. Feasibility study of particle-assisted laser ablation of brain tumors in orthotopic canine model. Cancer Res. 2009; 69:1659–1667. [PubMed: 19208847]
20. Day ES, Thompson PA, Zhang L, Lewinski NA, Ahmed N, Drezek RA, Blaney SM, West JL. Nanoshell-mediated photothermal therapy improves survival in a murine glioma model. J Neurooncol. 2010
21. De Jong WH, Hagens WI, Krystek P, Burger MC, Sips AJ, Geertsma RE. Particle size-dependent organ distribution of gold nanoparticles after intravenous administration. Biomaterials. 2008; 29:1912–1919. [PubMed: 18242692]
22. Terentyuk GS, Maslyakova GN, Suleymanova LV, Khlebtsov BN, Kogan BY, Akchurin GG, Shantrocha AV, Maksimova IL, Khlebtsov NG, Tuchin VV. Circulation and distribution of gold nanoparticles and induced alterations of tissue morphology at intravenous particle delivery. J Biophotonics. 2009; 2:292–302. [PubMed: 19434616]
23. Sonavane G, Tomoda K, Makino K. Biodistribution of colloidal gold nanoparticles after intravenous administration: effect of particle size. Colloids Surf B Biointerfaces. 2008; 66:274–280. [PubMed: 18722754]
24. Lasagna-Reeves C, Gonzalez-Romero D, Barria MA, Olmedo I, Clos A, Sadagopa Ramanujam VM, Urayama A, Vergara L, Kogan MJ, Soto C. Bioaccumulation and toxicity of gold nanoparticles after repeated administration in mice. Biochem Biophys Res Commun. 393:649–655. [PubMed: 20153731]
25. Hynynen K, McDannold N, Vykhodtseva N, Jolesz FA. Non-invasive opening of BBB by focused ultrasound. Acta Neurochir Suppl. 2003; 86:555–558. [PubMed: 14753505]

26. McDannold N, Vykhodtseva N, Raymond S, Jolesz FA, Hynynen K. MRI-guided targeted blood-brain barrier disruption with focused ultrasound: histological findings in rabbits. Ultrasound Med Biol. 2005; 31:1527–1537. [PubMed: 16286030]
27. Mesiwala AH, Farrell L, Wenzel HJ, Silbergeld DL, Crum LA, Winn HR, Mourad PD. High-intensity focused ultrasound selectively disrupts the blood-brain barrier in vivo. Ultrasound Med Biol. 2002; 28:389–400. [PubMed: 11978420]
28. Hynynen K, McDannold N, Sheikov NA, Jolesz FA, Vykhodtseva N. Local and reversible blood-brain barrier disruption by noninvasive focused ultrasound at frequencies suitable for trans-skull sonications. Neuroimage. 2005; 24:12–20. [PubMed: 15588592]
29. Hynynen K, McDannold N, Vykhodtseva N, Jolesz FA. Noninvasive MR imaging-guided focal opening of the blood-brain barrier in rabbits. Radiology. 2001; 220:640–646. [PubMed: 11526261]
30. Sheikov N, McDannold N, Sharma S, Hynynen K. Effect of focused ultrasound applied with an ultrasound contrast agent on the tight junctional integrity of the brain microvascular endothelium. Ultrasound Med Biol. 2008; 34:1093–1104. [PubMed: 18378064]
31. Kinoshita M, McDannold N, Jolesz FA, Hynynen K. Noninvasive localized delivery of Herceptin to the mouse brain by MRI-guided focused ultrasound-induced blood-brain barrier disruption. Proc Natl Acad Sci U S A. 2006; 103:11719–11723. [PubMed: 16868082]
32. Choi JJ, Wang S, Tung YS, Morrison B 3rd, Konofagou EE. Molecules of various pharmacologically-relevant sizes can cross the ultrasound-induced blood-brain barrier opening in vivo. Ultrasound Med Biol. 2010; 36:58–67. [PubMed: 19900750]
33. Treat LH, McDannold N, Vykhodtseva N, Zhang Y, Tam K, Hynynen K. Targeted delivery of doxorubicin to the rat brain at therapeutic levels using MRI-guided focused ultrasound. Int J Cancer. 2007; 121:901–907. [PubMed: 17437269]
34. Liu HL, Chang H, Chen WS, Shih TC, Hsiao JK, Lin WL. Feasibility of transrib focused ultrasound thermal ablation for liver tumors using a spherically curved 2D array: a numerical study. Med Phys. 2007; 34:3436–3448. [PubMed: 17926945]
35. Liu HL, Hua MY, Yang HW, Huang CY, Chu PC, Wu JS, Tseng IC, Wang JJ, Yen TC, Chen PY, Wei KC. Magnetic resonance monitoring of focused ultrasound/magnetic nanoparticle targeting delivery of therapeutic agents to the brain. Proc Natl Acad Sci U S A. 107:15205–15210. [PubMed: 20696897]
36. Chen PY, Liu HL, Hua MY, Yang HW, Huang CY, Chu PC, Lyu LA, Tseng IC, Feng LY, Tsai HC, Chen SM, Lu YJ, et al. Novel magnetic/ultrasound focusing system enhances nanoparticle drug delivery for glioma treatment. Neuro Oncol. 12:1050–1060. [PubMed: 20663792]
37. Lin CY, Liu TM, Chen CY, Huang YL, Huang WK, Sun CK, Chang FH, Lin WL. Quantitative and qualitative investigation into the impact of focused ultrasound with microbubbles on the triggered release of nanoparticles from vasculature in mouse tumors. J Control Release. 146:291–298. [PubMed: 20621645]
38. Raymond SB, Treat LH, Dewey JD, McDannold NJ, Hynynen K, Bacskai BJ. Ultrasound enhanced delivery of molecular imaging and therapeutic agents in Alzheimer's disease mouse models. PLoS One. 2008; 3:e2175. [PubMed: 18478109]
39. Jordao JF, Ayala-Grosso CA, Markham K, Huang Y, Chopra R, McLaurin J, Hynynen K, Aubert I. Antibodies targeted to the brain with image-guided focused ultrasound reduces amyloid-beta plaque load in the TgCRND8 mouse model of Alzheimer's disease. PLoS One. 5:e10549. [PubMed: 20485502]
40. Chithrani BD, Chan WC. Elucidating the mechanism of cellular uptake and removal of protein-coated gold nanoparticles of different sizes and shapes. Nano Lett. 2007; 7:1542–1550. [PubMed: 17465586]
41. Chithrani BD, Ghazani AA, Chan WC. Determining the size and shape dependence of gold nanoparticle uptake into mammalian cells. Nano Lett. 2006; 6:662–668. [PubMed: 16608261]
42. Jiang W, Kim BY, Rutka JT, Chan WC. Nanoparticle-mediated cellular response is size-dependent. Nat Nanotechnol. 2008; 3:145–150. [PubMed: 18654486]
43. Chopra R, Curiel L, Staruch R, Morrison L, Hynynen K. An MRI-compatible system for focused ultrasound experiments in small animal models. Med Phys. 2009; 36:1867–1874. [PubMed: 19544806]

44. Thorne RG, Nicholson C. In vivo diffusion analysis with quantum dots and dextrans predicts the width of brain extracellular space. Proc Natl Acad Sci U S A. 2006; 103:5567–5572. [PubMed: 16567637]

45. Niidome T, Yamagata M, Okamoto Y, Akiyama Y, Takahashi H, Kawano T, Katayama Y, Niidome Y. PEG-modified gold nanorods with a stealth character for in vivo applications. J Control Release. 2006; 114:343–347. [PubMed: 16876898]

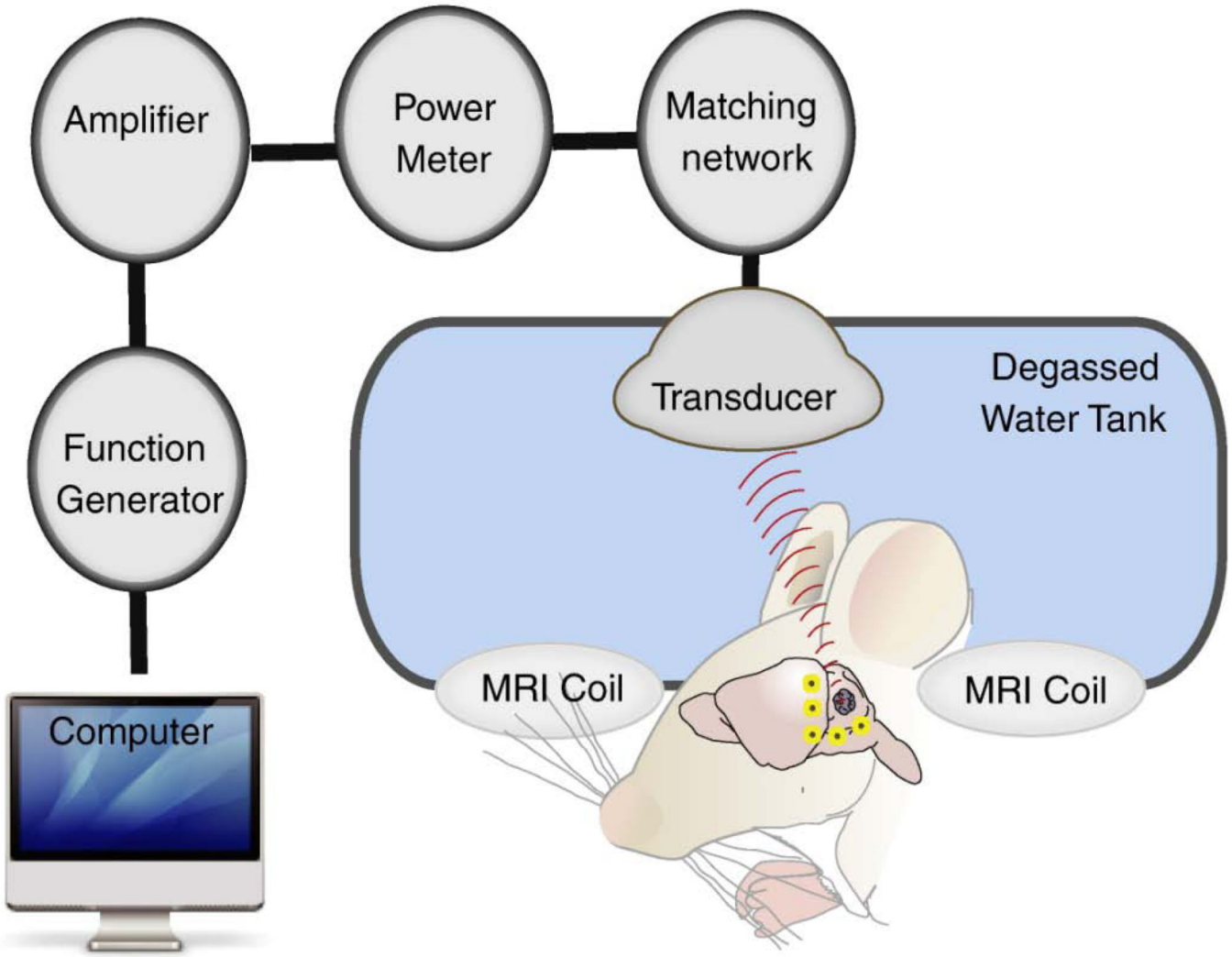

Figure 1. Schematic representation of the focused ultrasound system

Animal was placed supine with part of the skull submerged in a water tank. Transcranial ultrasound was then delivered to the right hemisphere. MRI was employed to confirm BBB disruption.

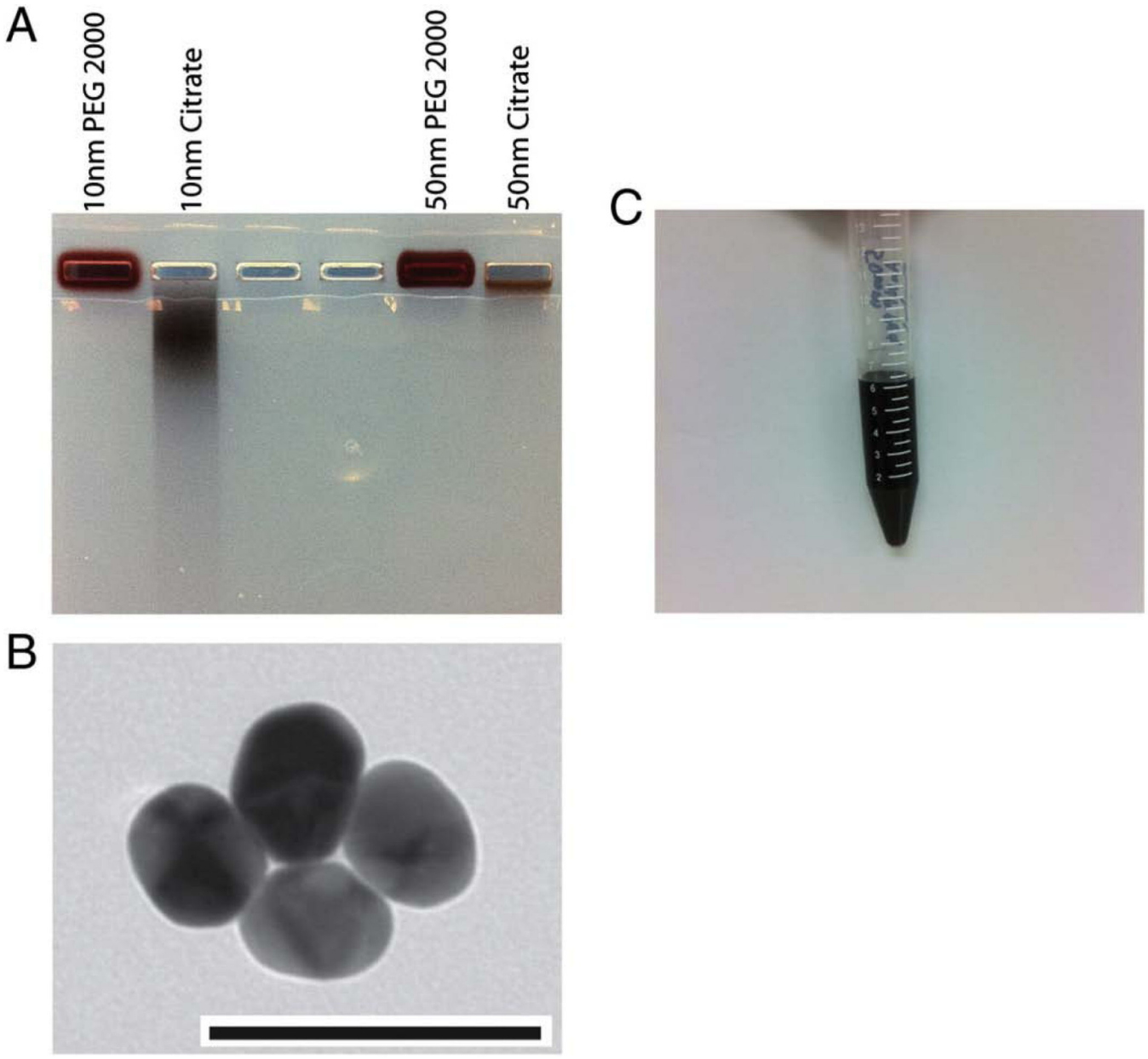

Figure 2. Characterization of AuNP

(A) Agarose gel (1%) electrophoresis of PEG and citrate stabilized AuNPs. PEG stabilized AuNPs did not demonstrate any mobility on the gel, whereas citrate stabilized particles migrated. (B) Transmission electron micrographs demonstrating spherical AuNPs (scale bar 100 nm). (C) Vial demonstrating the reddish brown coloration of 50 nm PEG AuNP.

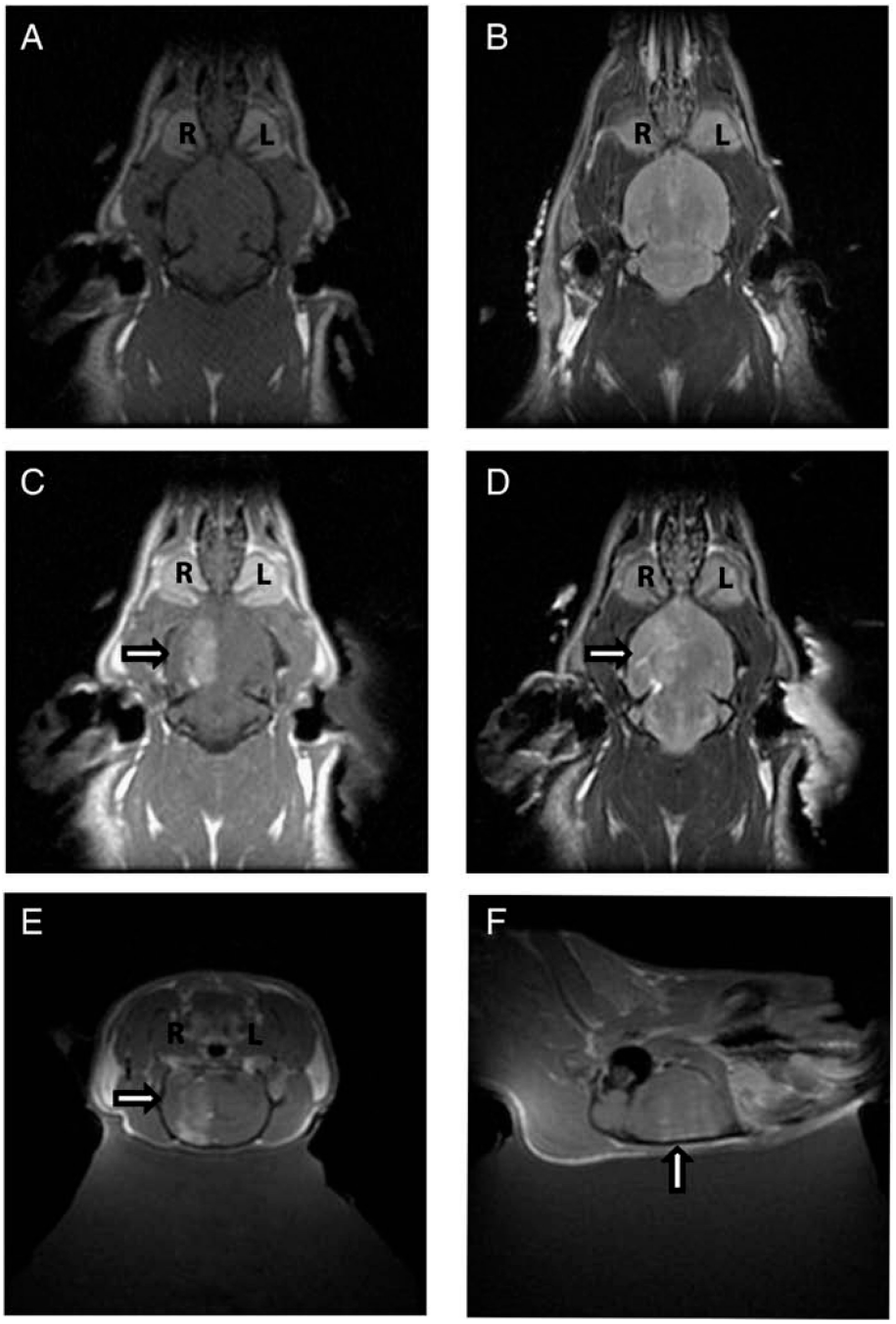

Figure 3. Magnetic resonance imaging (MRI) demonstrating disruption of BBB by MRgFUS

(A) Contrast enhanced axial T1-weighted images prior to MRgFUS does not show extravasation of gadolinium. (B) T2-weighted axial image prior to MRgFUS shows no increased signal. (C) Contrast enhanced axial T1-weighted images following MRgFUS shows extravasation (arrow) of gadolinium in the right hemisphere (R) but not the left hemisphere (L) suggesting BBB disruption. (D) T2-weighted axial images following MRgFUS shows increased T2 signal (arrow) corresponding to area of BBB disruption in the right hemisphere (R). Contrast enhanced coronal (E) and sagittal (F) T1-weighted images

following MRgFUS show extravasation of gadolinium (arrow) in the right hemisphere confirming BBB disruption.

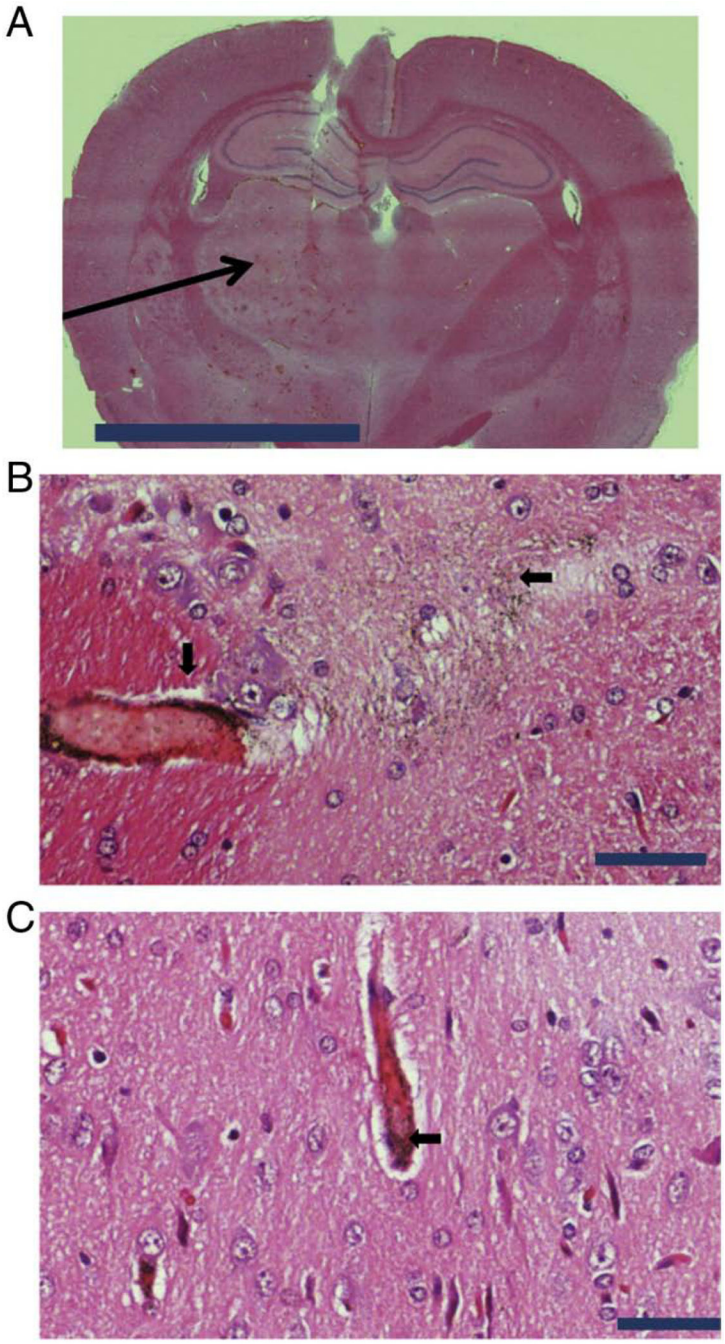

Figure 4. CNS localization of AuNP following of BBB disruption by MRgFUS

(A) H&E histology of coronal section of the right and left frontal lobes. The area (arrow) of BBB disruption by MRgFUS within the right frontal lobe is shown (scale bar 50,000 μm). (B) Demonstration (arrows) of peri-vascular and brain parenchyma localization of AuNP by silver enhancement and H&E histology within the right frontal lobe of CNS following MRgFUS. AuNP can be seen up to distances of 150 μm from initial site of BBB disruption (scale bar 50 μm). (C) Demonstration (arrow) of intra-vascular localization of AuNP by silver enhancement and H&E histology within the left frontal lobe of CNS in the absence of

MRgFUS. There was evidence of brain parenchyma (CNS) localization in left frontal lobe (scale bar 50 μm).

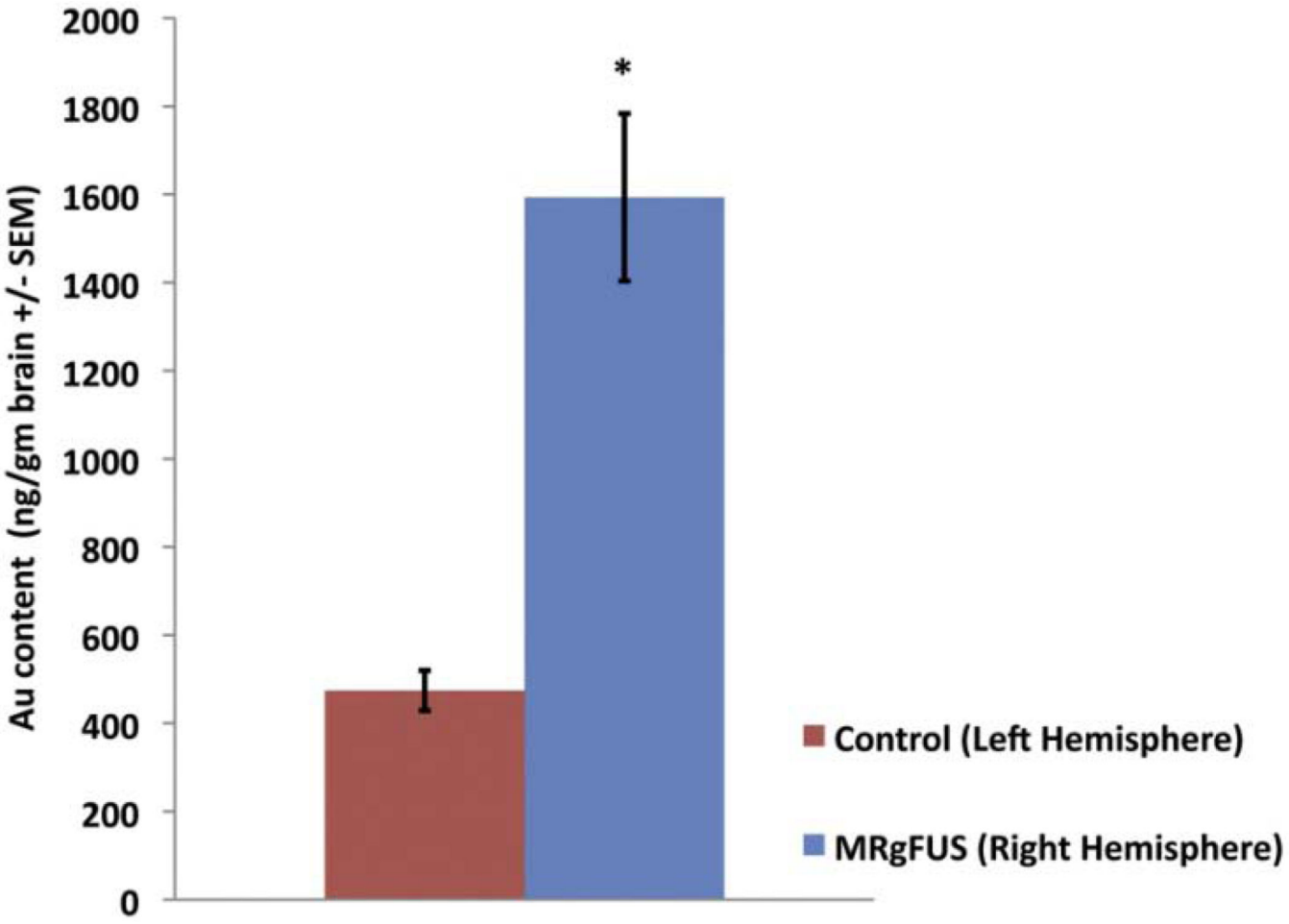

Figure 5. Enhanced CNS biodistribution of AuNP 2 hr following MRgFUS

Following tail vein injection of AuNPs, the FUS sonicated right hemisphere had a 336% enhanced uptake in comparison to the non-sonicated left hemisphere (n=5, P = 0.007). Error bars are standard error of the mean.

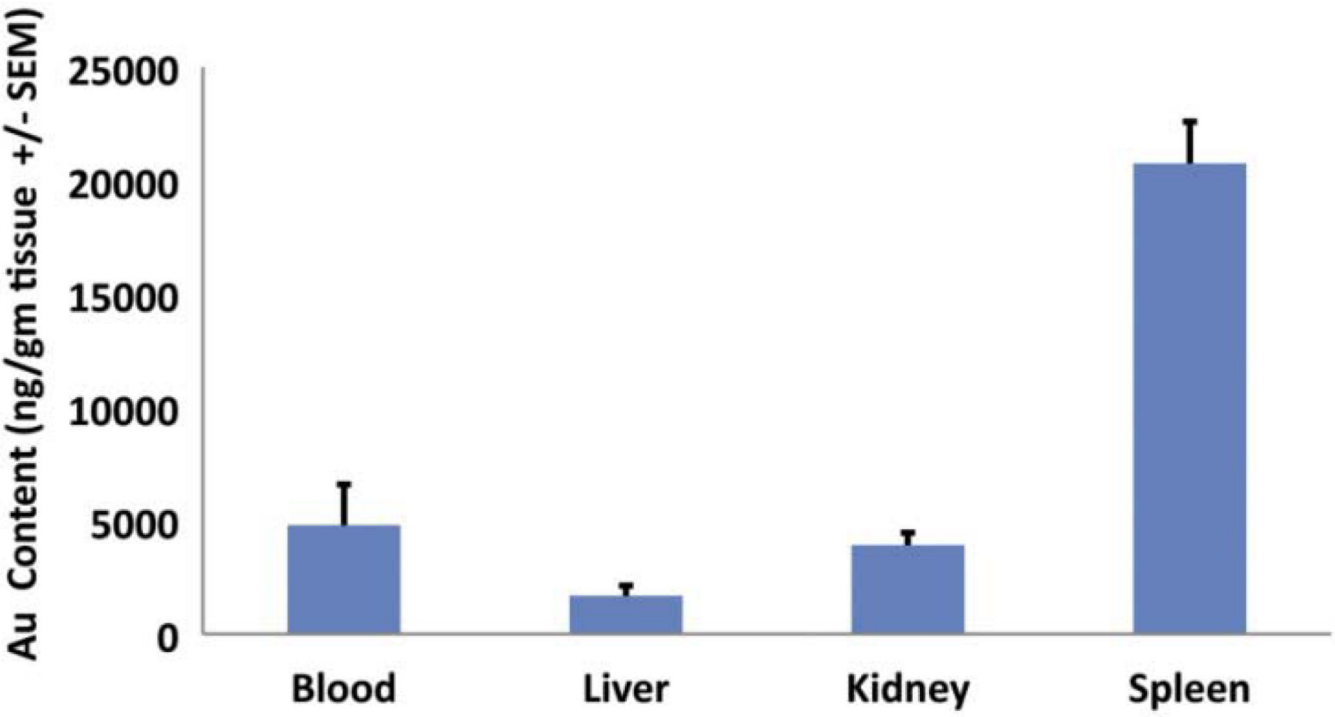

Figure 6. Biodistribution of AuNP outside the CNS 2 hr following MRgFUS

The largest amount of AuNPs following tail vein injection was noted in the spleen, followed by kidney, blood and liver. Error bars are standard error of the mean (n=5, $P < 0.001$ between group ANOVA).